CrossMark

Characterisation and modelling of in-plane springback in a commercially pure titanium (CP-Ti)

S. Khayatzadeh[1,*] , M. J. Thomas[2], Y. Millet[3], and S. Rahimi[1]

[1] *Advanced Forming Research Centre (AFRC), University of Strathclyde, 85 Inchinnan Drive, Inchinnan, Renfrew, Glasgow PA4 9LJ, UK*
[2] *TIMET UK Ltd., Witton, Birmingham B6 7UR, UK*
[3] *TIMET SAVOIE, 62 Avenue Paul Girod, 73400 Ugine, France*

ABSTRACT

Effective prediction of springback during sheet metal forming is critically important for automotive and aerospace industries, especially when forming metals with high strength-to-weight ratio such as titanium. This requires materials mechanical data during plastic deformation and their dependencies on parameters like strain, strain rate and sample orientation. In this study, springback is quantified experimentally as elastic strain recovery, degradation in Young's modulus and inelastic strain recovery on unloading in a commercially pure titanium type 50A (CP-Ti-50A). The results show strain rate-dependent anisotropic mechanical behaviours and a degradation in Young's modulus with increased level of plastic deformation. The level of degradation in Young's modules increases gradually from 13% for samples parallel to the rolling direction (RD) to 20% for those perpendicular to the RD. A measurable nonlinear strain recovery was also observed on unloading that is orientation dependent. The level of springback is characterised as the sum of elastic recovery and the contributions from both the degradation in Young's modulus and anelastic strain recovery. It is shown that the Chord modulus can estimate springback with a reasonable accuracy taking into consideration the elastic strain recovery, degradation in Young's modulus and anelastic strain recovery.

Introduction

Springback is a strain recovery in a formed product following a forming process [1] that often causes deviation from a desired geometry. In addition to the geometrical non-conformance, springback also changes the status of strain and stress in a deformed material following the tool's (e.g. punch) removal [2–4]. Springback is one of the major engineering problems associated with parts manufacturing, especially in sheet metal forming processes due to the small thickness of the sheet material. This is even more pronounced for high-strength metals such as titanium and its alloys that are used predominantly

⚫ Springer

in aerospace industry, due to their high strength-to-weight ratio [5]. Accurate prediction of springback for such metals is a challenge, particularly for parts with complex geometries. An extensive body of the literature exists on studying springback in different materials, where the origin of springback is linked to the changes in materials mechanical properties and responses during plastic deformation [1, 6–12].

Representing material's elastic behaviour as a linear trend (i.e. Young's modulus) is one of the sources of uncertainties when modelling springback. A study reported by Chen et al. [6] on 26 diverse commercial sheet alloys showed that no finite linear trend can be observed in the elastic region during loading of these alloys. In contrast, a consistency in the data was observed for nonlinearity throughout the transition region from elastic to plastic, starting from very low stress levels far below the yield point. Therefore, considering elastic behaviour as a linear curve by using a single value for Young's modulus to describe the elastic region can potentially generate significant uncertainties in determination of springback. This is even more pronounced during unloading compared to loading [1, 5, 7–9, 13–15].

Earlier studies [1, 7, 8, 10, 11, 13–17] show a degradation in Young's modulus as a function of the level of plastic deformation for different alloys. This has usually been shown by comparing the initial elastic modulus, characterised using standard methods, at no plastic strain to those measured after various levels of plastic strain through interrupted tensile tests, consisting of a series of loading–unloading–loading steps on a same sample [5]. In addition to progressive degradation in Young's modulus as a function of plastic deformation, Luo and Ghosh [1] have shown that following plastic deformation in deep drawing of quality special killed (DQSK) steel, an inelastic nonlinear strain recovery occurs making the total strain recovery that is greater than the value expected on the basis of considering degraded single value for elasticity. This form of visco-plastic strain recovery is known as "anelastic" strain which is time rate dependent, and these dependencies have not been reported previously [1, 8, 13]. It was shown that higher levels of plastic deformation reduce Young's modulus significantly, though increases Poisson's ratio [1]. Different methodologies exist to study degradation in Young's modulus as a function of plastic deformation, such as interrupted uniaxial [1, 7, 8, 13–15, 18] and biaxial

loading–unloading–loading tensile tests [19, 20], and pre-strained three-point bending tests [19, 21–23]. The former is the most reported method used for detailed characterisation of elastic modulus during plastic deformation [1, 7, 8, 10, 11, 13–17]. Despite the intensive application of interrupted tensile test technique, it has been argued that the pre-strained three-point bending test provides measurement of degradation in elastic modulus during plastic deformation more accurately [19]. A comparative study of uniaxial, biaxial and three-point bending test methods was carried out by Xue et al. [19] on three types of dual-phase steels (i.e. DP500, DP600 and DP780), and the highest and lowest initial elastic modulus were those of uniaxial and biaxial testing methods, respectively, and that of the three-point bending tests were in between.

Degradation in elastic modulus by increasing the level of plastic deformation has been observed for different materials. Benito et al. [11] reported $\approx 8\%$ decrease in Young's modulus with 6% plastic deformation in pure iron deformed by drawing at room temperature, followed by a negligible increase in the Young's modulus (≈ 6 GPa) after further 3% deformation. In a study conducted on TRIP 700 steel by Mendiguren et al. [7], the Young's modulus is decreased by 20% after 12% plastic deformation, which raised an alarm on considering this significant change in the prediction of post-forming springback. The level of degradation is shown to vary for different materials. These differences were studied by Abvabi et al. [10] where the degradation was observed to be more pronounced for higher-strength steels compared to softer grades.

Springback is mainly known as elastic strain recovery, while various studies [5, 8, 9, 14, 18] conducted on steels and aluminium show springback as a combination of elastic and anelastic strain recoveries. It is a common practice to use the slope of the loading curve (i.e. Young's modulus) in each loading–unloading loop, to investigate the degradation in Young's modulus, using interrupted tensile test procedure [14, 15]. In this approach, the nonlinear strain recovery occurring during the unloading step was originally neglected; however, later studies considered the Chord modulus as a criterion to overcome this source of uncertainty for springback investigation [5–7, 9, 10, 13, 14, 24]. Chord modulus is the slope of a straight line connecting the start and the end points of unloading step of each loading–

unloading cycle of interrupted tensile tests. It can be used as a mean value for estimating springback including elastic strain recovery, degradation in Young's elastic modulus and nonlinear strain recovery [5]. Chord modulus has been used in springback prediction models based on finite element analyses [5, 10, 14], and the results were more closer to the experimentally measured springback. This was generally done by substituting the elastic modulus with changes in Chord modulus versus the level of applied plastic deformation. Also, as similar as to the degradation in Young's elastic modulus, a degradation in Chord modulus is observed with increasing plastic deformation [5, 8, 14].

The anelastic strain recovery can be significantly high, as for instance $\approx 20\%$ of the total strain recovery is measured in TRIP steel [18]. Sun et al. [14] investigated the strain recovery following plastic deformation, by describing the strain as a quasi-plastic–elastic (QPE) phenomenon that has resulted from a combination of elastic, plastic and QPE deformations. A significant improvement was achieved in predicting springback using this model in dual-phase steel [14]. It was shown that a significant magnitude of nonlinear strain recovery occurred in addition to the elastic strain recovery following unloading, taking into consideration the degradation in elastic modulus as a function of plastic strain [14].

During sheet metal forming process, an abundance of plastic strain is introduced to a deformed part at different strain rates. For complex geometries, the actual strain rate may vary for different areas of the part [25]. Previous reports [15, 26, 27] suggest that springback can be drastically influenced by strain rate and work hardening behaviours of the material. This was clearly shown for two different aluminium alloys of type 2024-T3 and type 2024-O, where the springback for the later exhibited much lower sensitivity to strain rate compared to that of the former [27]. An additional study [26] also showed that springback in commercially pure titanium is sensitive to strain rate. Despite the importance of the influence of strain rate on springback, and the locational dependency of strain rate throughout a part during sheet forming processes, there is still lack of understanding of the overall effect on springback.

Additionally, in anisotropic materials springback behaviour varies for different orientations of a part due to the directional dependency of the mechanical properties [28]. Few studies have attempted to take the anisotropic mechanical properties into an account when estimating springback [7, 28–30]. It was concluded that the springback magnitude was dependent on the orientation of the investigated sample with respect to the rolling direction of the original sheet.

Establishing a relationship between springback and an appropriate material model is vitally important, to estimate springback more effectively. This requires a clear understanding of changes in material's behaviours, such as elastic modulus, with plastic deformation, as well as the elastic and anelastic strain recovery behaviours upon unloading. This paper aims to present a clear understanding of the evolution of Young's modulus as a function of plastic deformation, and the elastic and anelastic strain recovery behaviours in a commercially pure titanium type 50A. The purpose is to gain a thorough understanding of mechanical properties in different directions to quantify the influence of plastic deformation on Young's modulus and anelastic strain recovery that are both required in springback prediction models.

Experimental procedure

Material and microstructure characterisation

The material investigated in this study is an uncoated cold rolled sheet of commercially pure titanium grade 50A (CP-Ti50A) with a thickness of 1.6 mm. This was supplied by TIMET in a form of sheets with 1.6 mm $\times$ 1 m $\times$ 2 m ($T \times W \times L$) dimensions. The specimens for uniaxial tensile tests were extracted from the as-received sheets using electrical discharge machining (EDM) with their lengths along three orientations of 0°, 45° and 90° angles to the rolling direction (RD), to investigate the extent of material's mechanical anisotropy. The samples were manufactured based on ASTM E8/EM8-11 [31], with gauge length and width dimensions of 57 and 12.5 mm, respectively.

Electron backscatter diffraction (EBSD) was used for microstructure characterisation and quantification of texture in the as-received material. For the EBSD analysis, samples were cut from the as-received sheet's cross section, parallel and perpendicular to the RD, and mechanically ground by silicon carbide

(SiC) and polished by 6- and 1-µm lubricate diamond paste, successively. The mirror-finished samples were then electro-polished at ambient temperature for 60 s at 30 V in Struers' electrolyte A3, to remove approximately 20- to 30-µm material from the mechanically polished surface. The acquisition of EBSD maps was carried out using a fully automated AZtec HKL Advanced (plus C5 Prem) Nordlys Max 2 EBSD system interfaced to a FEI Quanta-650 field-emission gun scanning electron microscope, with an accelerating voltage of 20 kV and a 100-µm-diameter aperture. The acquisition time was set to 60 ms, collecting at least 2 frames for each point. High-resolution orientation maps with 0.5-µm step size and 550 µm × 500 µm area each have been collected from both sample orientations (i.e. cross sections parallel (ND–RD) and perpendicular (ND–TD) to the RD). ND and TD, respectively, stand for the normal direction and transverse direction. In all cases, a minimum of 88% of the scanned areas were indexed.

Uniaxial tensile testing

Uniaxial tensile tests were conducted using a Zwick Roell Z250 machine to examine the mechanical properties in different directions of the as-received material. The standard tensile tests were carried out under three different strain rates of 0.002, 0.01 and 0.1 s^{-1} for each sample orientation (i.e. 0°, 45° and 90° to the RD). Each test condition was repeated twice (i.e. total of 18 experiments) for each sample orientation. An external MTS-type extensometer, capable of measuring displacement in two directions of length (L) and width (W), was employed to measure the changes in dimensions along and across the gauge length of the samples during testing. True stress and true strain were computed from the engineering data set, under an assumption that the sample's volume remains constant after deformation in tension.

Interrupted tensile testing

A set of interrupted tensile tests consisting of several stages of loading–unloading–loading loops were conducted on the standard tensile samples with their lengths at 0°, 45° and 90° to the RD, under the same parameters (e.g. strain rate) as those of the standard tensile experiments. These tests were carried out using the same tensile test machine (i.e. Zwick/Roell)

as that of the uninterrupted standard tensile tests in displacement control mode in which a number of deformation steps (i.e. loading and unloading) were applied. For each loading and unloading loop, the sample was loaded at displacement control condition up to a predefined target strain and then unloaded to a nonzero 50 N load to ensure that the sample is not subjected to compression on unloading. For each sample orientation and strain rate, two tests were performed with different numbers of loading–unloading loops, one with 5% increment in strain in each step and the other with 4%. This was to understand the potential dependency of the measured parameters such degradation in Young's modulus, on the number of loops during interrupted tensile testing.

For each sample, displacement along the gauge length was measured during the test using a clip-on extensometer, as well as by digital image correlation (DIC) method. The difference between the results of both displacement measurement techniques was very small (i.e. maximum of 0.3%). For each loading–unloading loop, Young's modulus was measured during loading, as similar as that for an uninterrupted tensile test, based on ASTM standard [32]. The Chord modulus was also calculated for each unloading–loading loop using the slope of a line connecting the start and end points of an unloading step. This was also done to study the degradation in Chord modulus with a progress of plastic strain, similar to that of Young's modulus.

The surface displacement along and across the gauge length for each sample was mapped during the test using DIC technique capable of mapping the in-plane and out-of-plane displacements during loading–unloading cycles. Images of the sample surface were recorded using LaVision's MX4M digital cameras installed on a Zeiss Discovery.V12 3D stereo microscope. The time interval between observations varied from 0.04 to 0.1 s throughout the tests, depending on the strain rate. The obtained images were analysed by LaVision DaVis Image Correlation software (version 8.3.0) to evaluate in-plane 2D displacement map using a 60 × 60 pixel interrogation windows with 30% overlap. In these tests, one pixel is equivalent to 39 µm. Displacements were therefore measured on the surface at positions with grid spacing of 1.6 mm in all cases.

Residual stress measurements

Surface and through thickness residual stress were measured on both sides of the as-received sheet and within the gauge length of the specimens extracted for tensile tests. The purpose of these measurements was to understand the status of stress in the as-received material and after extracting the specimens, prior to the tensile experiments. The surface residual stress was measured using a Proto laboratory X-Ray Diffraction (LXRD) stress diffractometer and $\sin^2\psi$ method [33]. The measurement points were along two directions of parallel to, and perpendicular to the RD for the as-received sheets, and longitudinal (along the length) and transverse (along the width) of the gauge length of tensile samples. The stresses were calculated from the strains of the {302} reflection plane at 148.7° Bragg angle. The stress uncertainty was obtained from the best fit to the $\sin^2\psi$ plot. For each point in both directions, 10 measurements with 3 s exposure time for each measurement were performed. A round collimator with 1 mm radius and eleven ψ-offset angles in the range of maximum $\pm$ 30° were employed.

The through thickness stress measurement was carried out using a PRISM hole-drilling system manufactured by Stresstech that measures surface displacement based on electronic speckle pattern interferometry (ESPI) using a monochromatic laser with 532 nm wavelength as a light source for illumination. The endmills used for these measurements were 1.8 mm titanium aluminium nitride (TiAlN)-coated drills. Images were recorded after each step increment, and subsequently, the surface displacement induced by material removal during drilling was measured. The measured displacements were then used for the calculation of residual stress assuming Young's modulus of 104, 109 and 117 GPa for samples at 0°, 45° and 90° angles to the RD, respectively. These values for Young's modulus were extracted from the standard tensile experiments carried out in this study. A Poisson's ratio of 0.3 was considered for all directions.

Results

Material's microstructure

The microstructure of the as-received CP-Ti sheet in the plane containing the normal (ND) and rolling directions (RD) and normal to the transverse direction (TD) is given in Fig. 1a and b, respectively, with IPF colouring with respect to the TD. The EBSD data show that the CP-Ti material has a twin-free microstructure with equiaxed grains in both ND–RD and ND–TD planes with a similar average grain size of 5.6 ± 3.5 μm (Fig. 1d) and a typical rolled α-Ti texture. The measured rolled α-Ti texture is a split (0001) basal texture with most c-axes inclined at an angle of $\pm$ (25°–35°) from the ND towards the TD and almost randomly oriented *a*-axis, as shown in {0001} and $\{10\bar{1}0\}$ pole figures in Fig. 1c. The maximum (0001) pole intensity of ~ 5.6 was observed at two symmetric positions of $\phi_1 = 0°$ and 180°, $\phi = 30°$ and ϕ_2 varied in the range of $0° \leq \phi_2 \leq 60°$. Euler angles ϕ_1, ϕ and ϕ_2 were defined with reference to the HCP crystal coordinates of the $[1\bar{1}00]$ = RD, $[2\bar{1}\bar{1}0]$ = TD and [0001] = ND.

Residual stress measurements

The surface and through thickness residual stress profiles measured on the titanium sheet in the as-received condition, prior to manufacturing of the tensile specimens, assessed by both XRD- and ESPI-based hole drilling, are shown in Fig. 2. The data show very low surface residual stress in the transverse direction (TD) and a small compressive (≈ -30 MPa) surface residual stress in the rolling direction (0° to the RD). On the other hand, the results of hole-drilling based on ESPI show higher levels of residual stress with depth, changing from -60 to 60 MPa for the TD and -80 MPa to 80 MPa for the RD. Figure 3 shows the results of residual stress measurements taken from both sides of the tensile samples, within the gauge length, at different orientations with respect to the RD. For each sample, 5 points along the gauge length were measured. The measured stresses along the length of all samples (Sxx), disregarding sample orientations (i.e. 0°, 45° and 90° to the RD), appear to be changing about 0 ± 20 MPa for both faces (Fig. 3b and c). Similarly, the stresses measured perpendicular to the lengths of the samples machined at 0° and 45° to the RD are about 0 ± 10 MPa for both faces; however, those of the samples machined at 90° to the RD are about 30 ± 10 MPa for face 1 and -40 ± 10 MPa for face 2 (Fig. 3b, c). These results suggest that the magnitudes of residual stress in the samples with their lengths at
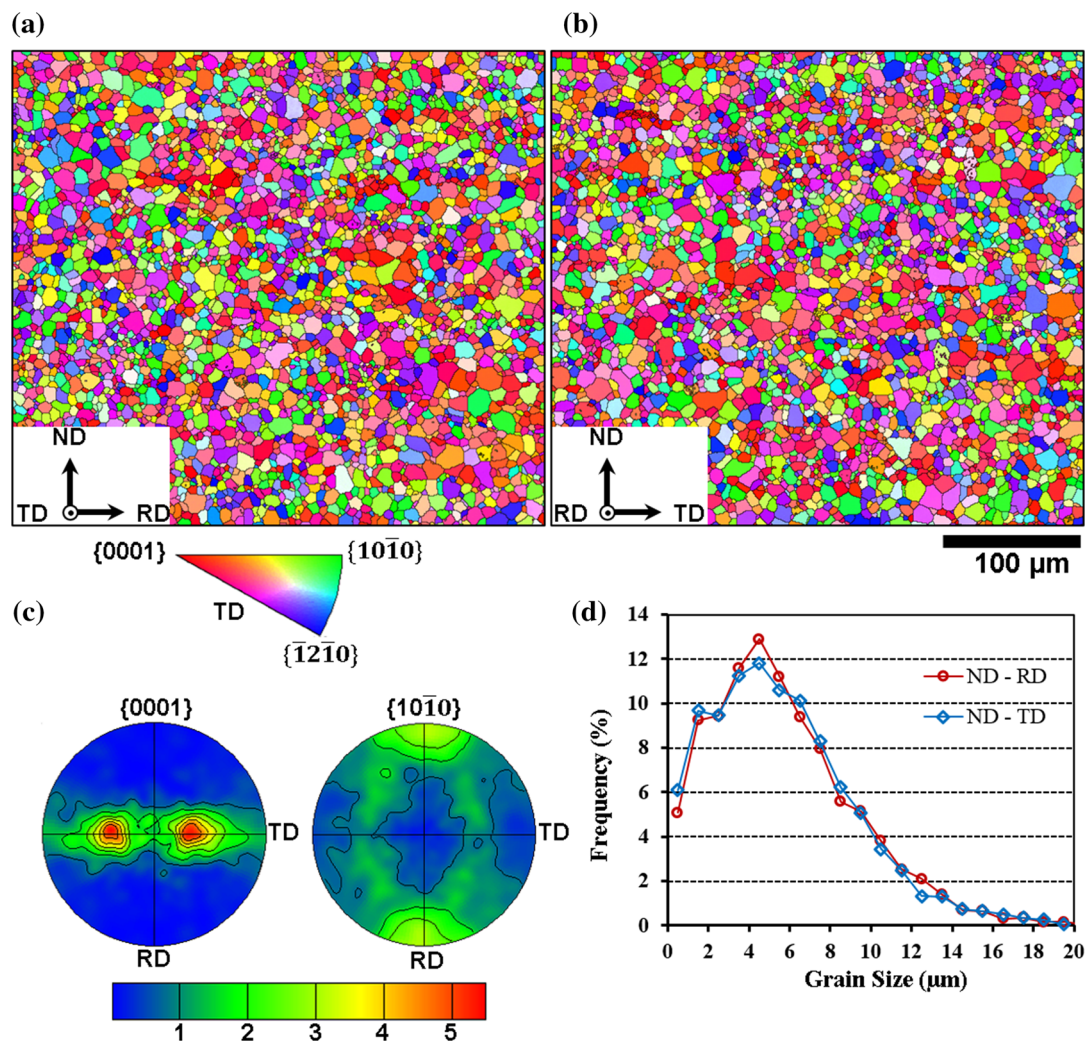
Figure 1 Microstructure characteristics of the as-received CP-Ti used in these investigations; **a** and **b,** respectively, show the EBSD orientation maps with IPF colouring with respect to the TD of the cross sections containing ND–RD and ND–TD (i.e. parallel and perpendicular to the RD), **c** corresponding $\{0001\}$ and $\{10\bar{1}0\}$ pole figures of the EBSD map shown in (**a**) and **d** grain size distributions of both the ND–RD and ND–TD cross sections evaluated from the EBSD maps.

90° to the RD are slightly higher compared to those oriented at 0° and 45° to the RD.

Anisotropic behaviour

Table 1 summarises the details of the results of standard tensile tests for three orientations of the as-received sheet (i.e. 0°, 45 ° and 90 ° to the RD), under different testing conditions. The gauge length displacement for each specimen was measured by both clip-on extensometer and DIC technique which their results were comparable and consistent. For each test, Young's modulus (E), yield stress ($\sigma_{0.2}$), ultimate tensile strength (σ_{uts}) and failure strain (ε_f) are

analysed. These data show that Young's modulus is not sensitive to strain rate ($\approx$ 1 GPa), for the same sample orientation. This is consistent with the results of several studies reported on the effect of strain rate on Young's modulus [1, 14, 15], where no noticeable changes were observed. However, a study by Leacok et al. [26] showed that the initial Young's modulus of commercially pure titanium increases with higher strain rates. Figure 4a, b, and c, respectively, shows the plots of true stress– true strain curves for samples at 0°, 45° and 90 ° to the RD obtained under different strain rates of 0.002, 0.01 and 0.1 s^{-1}. For each sample orientation, the yield stress is observed to be increased with an increase in the strain rate. Also, at
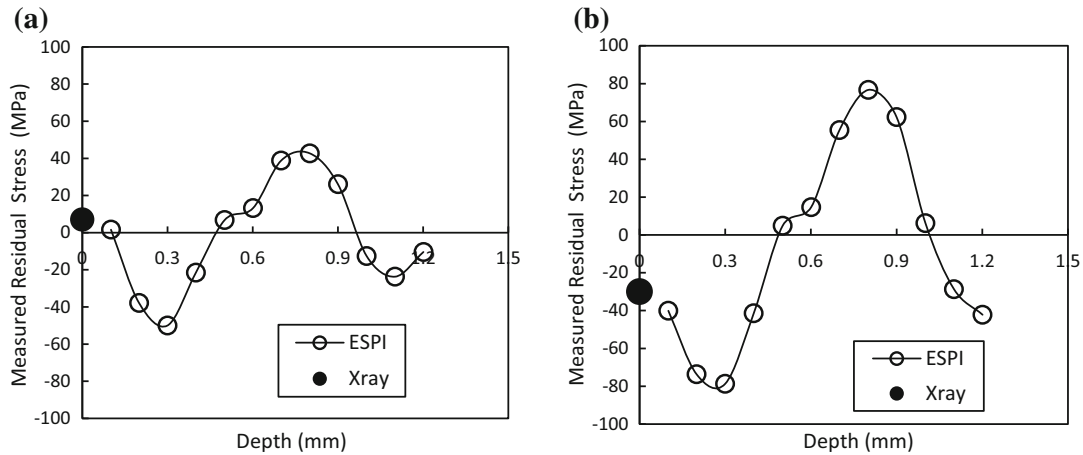
Figure 2 Surface and through thickness residual stress components measured by XRD- and ESPI-based hole drilling on the as-received Ti50A sheet. **a** Sxx-along TD and **b** Syy-along RD.

each strain rate, the yield stress is increased by changing the sample orientation from 0° to 90° with respect to the RD. For instance, under applied strain rate of 0.002 s^{-1}, the measured yield stress for the sample at 0° to the RD is ≈ 301 MPa, and that of the sample at 90° to the RD is ≈ 407 MPa. Similarly, the Young's modulus is increased by 10% with changing sample's orientation from 0° to 90° to the RD. The percentages of elongation of the samples with their lengths at 45° to the RD are higher, compared to those of the samples at 0° and 90° to the RD. However, the ultimate tensile strength (UTS) shows an opposite behaviour where the maximum value was measured for the samples at 0° to the RD and minimum value was measured for the samples at 45° to the RD. In general, the results of tensile experiments show that the material behaviour is strain rate dependent.

Figure 5a shows the full engineering stress–true strain curves for samples with different orientations to the RD, tested under a constant strain rate of 0.01 s^{-1}. It is apparent that the work hardening is reduced by changing the sample orientation from 0° to 90° to the RD. The stress–strain curves of the samples at 45° and 90° to the RD were following a similar trend, while that of the sample parallel to the RD (i.e. 0°) showed higher strain hardening rate. The data were fit in Hollomon's empirical equation shown in Eq. (1), to evaluate the strain hardening coefficients for different orientations [34].

$$\sigma = k(\varepsilon_p)^n \tag{1}$$

where σ is flow stress, ε_p is true plastic strain, k and n are material's constants known as strengths

constant and strain hardening exponent, respectively. The constants were computed for the experimental flow curves obtained for all three sample orientations (i.e. 0°, 45° and 90° to the RD) tested under strain rate of 0.01 s^{-1}. The constants are summarised in Table 2. These constants (i.e. K and n) were appeared to be orientation dependent. This is evident by comparing the K and n values computed for different sample orientations (see Table 2). Figure 5b emphasises on the elastic region and early stage of the plastic deformation of the results of standard tensile tests obtained for different sample orientations. A second yield point can be seen for samples at both 45° and 90° to the RD, though it is more pronounced for the latter (Fig. 5).

Effect of plastic deformation on elastic modulus

Figure 6a shows the results of two different cases of interrupted tensile tests with different numbers of loading–unloading loops, conducted on samples 0° to the RD and under a strain rate of 0.002 s^{-1}. The true stress–true strain data for a continuous standard tensile test obtained for the same sample orientation and similar condition are also provided for the aid of comparison. The interrupted tensile test trials include a test with 5% strain interval and another with 4% strain interval between each loading and unloading step. A similar trend has been observed for the results of both continuous and interrupted tests, and no obvious difference was seen between the results of interrupted tests with different strain intervals.
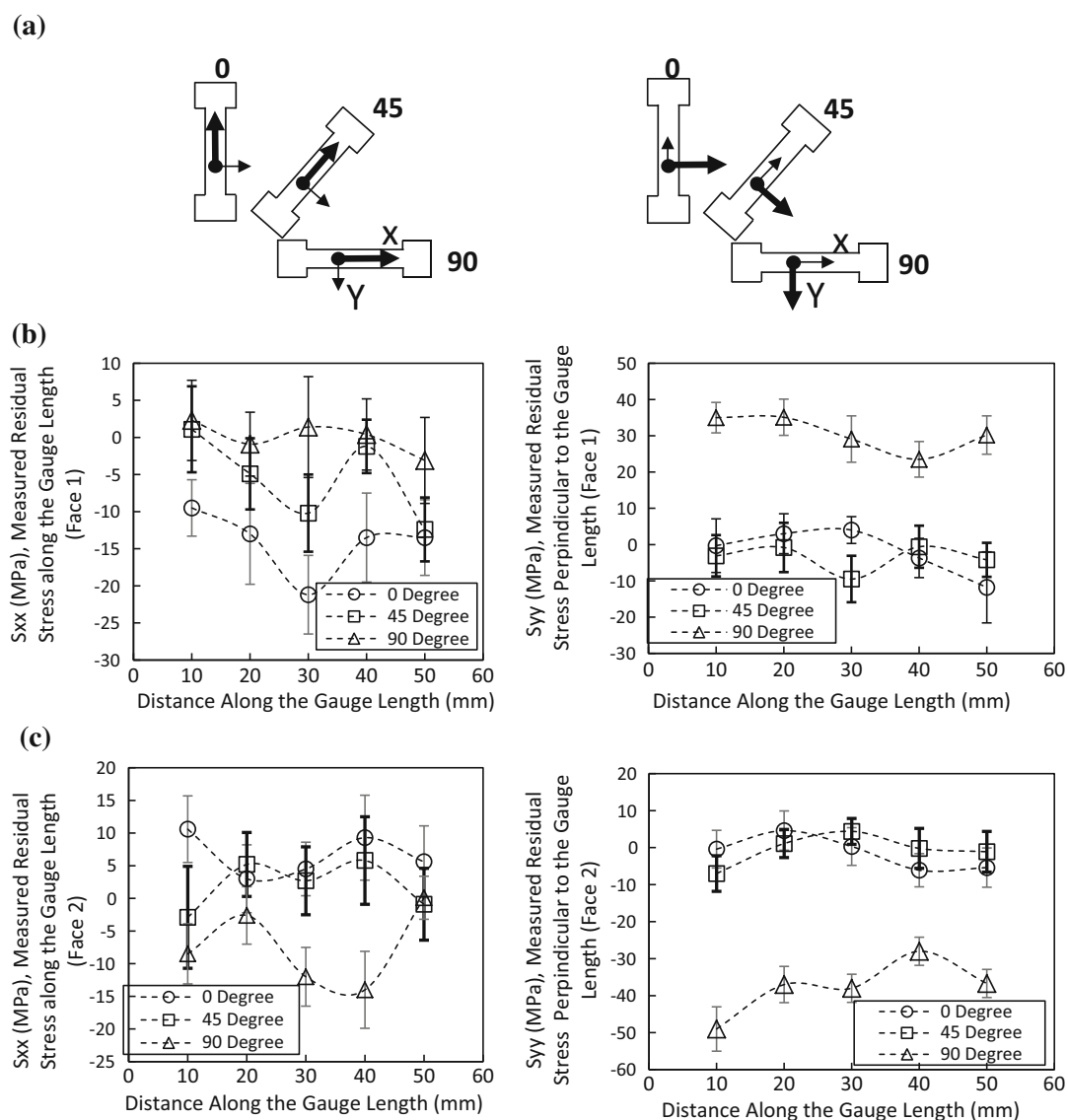
(a)

(b)

(c)

Figure 3 a Schematic illustration of the direction of tensile specimens with respect to the RD and the highlighted directions of the XRD stress measurements with bold arrows, **b** and **c** distribution of residual stresses along and perpendicular to the gauge length for face 1 and face 2, respectively.

Table 1 Details of mechanical properties obtained from the standard tensile tests conducted on samples at different orientations to the RD of the as-received sheet

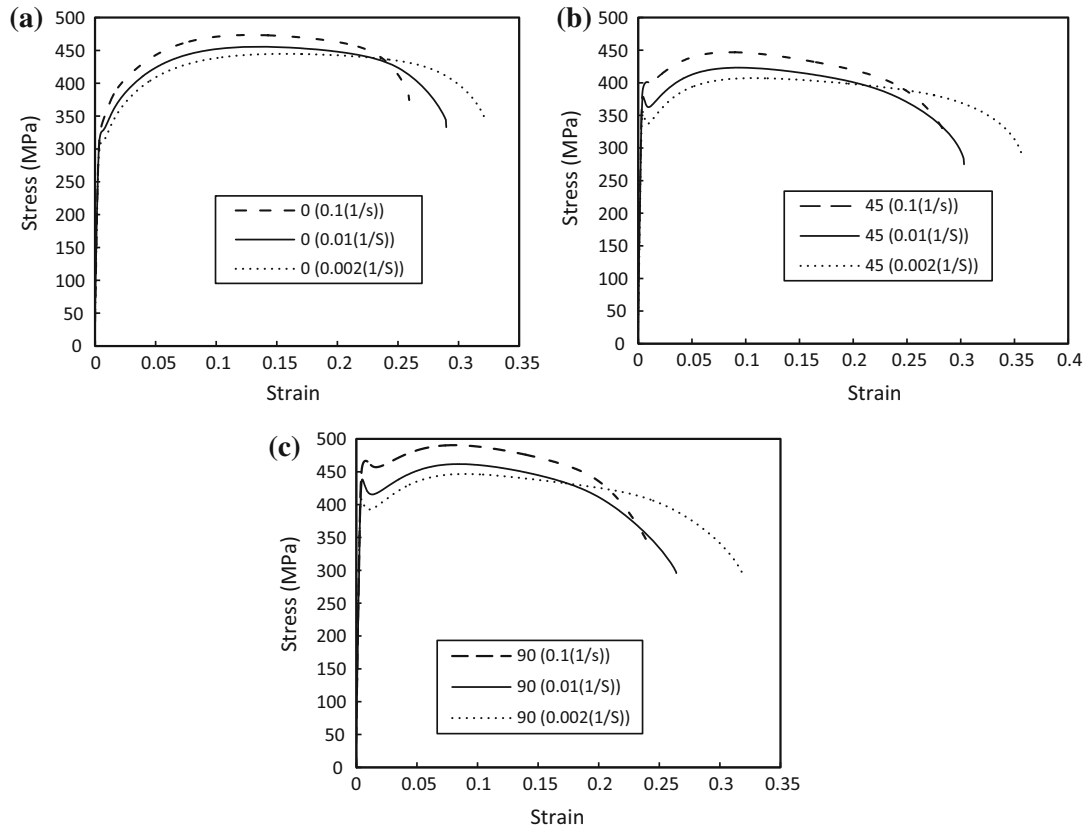| Direction of sample	0°			45°			90°		
Strain rate (1/sec)	0.002	0.01	0.1	0.002	0.01	0.1	0.002	0.01	0.1
E (GPa)	102.0	104.7	103.7	109.8	110.3	110.2	117.8	119.2	119
Elongation, (ε_f) %	28	26	23	31	27	25	28	24	22
0.2% yield (MPa), $(\sigma_{0.2})$	301	309	332	342	367	394	407	418	452
Ultimate tensile strength (MPa), (σ_{uts})	452	463	473	414	432	449	446	466	486

Figure 4 Engineering stress–strain curves measured on CP-Ti50A samples under different strain rates of 0.002, 0.01 and 0.1 s^{-1}, for samples oriented at **a** 0°, **b** 45° and **c** 90° to the RD.
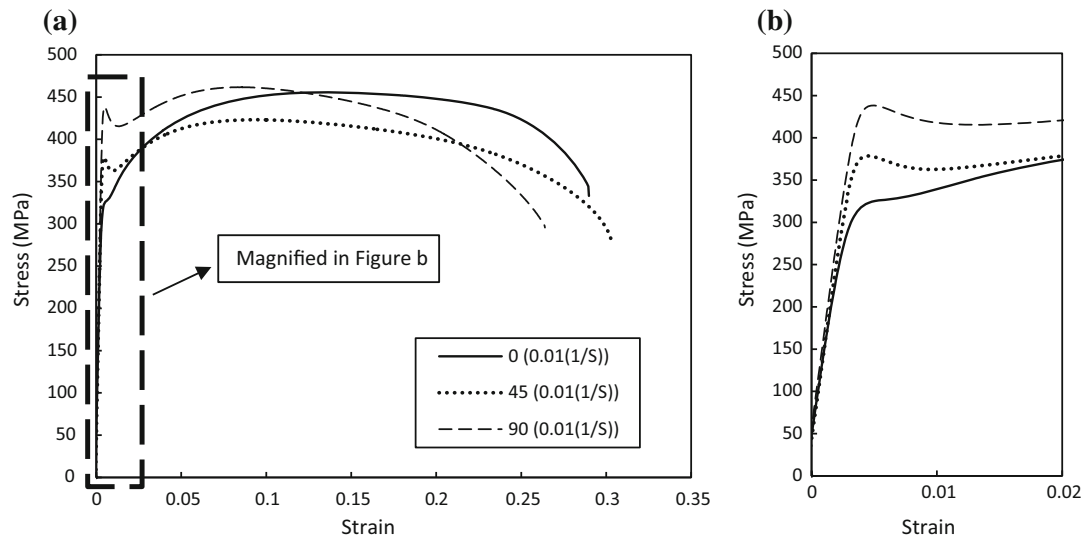

Figure 5 Engineering stress–strain curves obtained from CP-Ti50A samples with different orientations of 0°, 45° and 90° to the RD, tested under a constant strain rate of 0.01 s^{-1}: **a** full tests and **b** magnified elastic region highlighted in (**a**).

Figure 6b shows the results of interrupted tensile tests on samples at 90° to the RD, under different strain rates. A consistency can be observed between the two testing methods, when comparing the results of interrupted tensile tests (Fig. 6b) with those of the

Table 2 Material's constants computed by fitting the measured stress–strain curves to Hollomon's empirical equation for different sample orientations of the as-received sheet, tested under 0.01 s^{-1} strain rate

	0°	45°	90°
k	685	559	586
n	0.1451	0.09046	0.0731

continuous standard tensile tests (Fig. 4) under different strain rates.

The elastic regions of the loading stages of all the loading–unloading cycles of the interrupted tensile tests, carried out on two sample orientations of 0° and 90° to the RD under 0.01 s^{-1} strain rate, are superimposed by translating them to a common coordinate, as shown in Fig. 7. The slope of stress–strain curve in the elastic region (i.e. Young's modulus) is reducing with an increase in the level of plastic
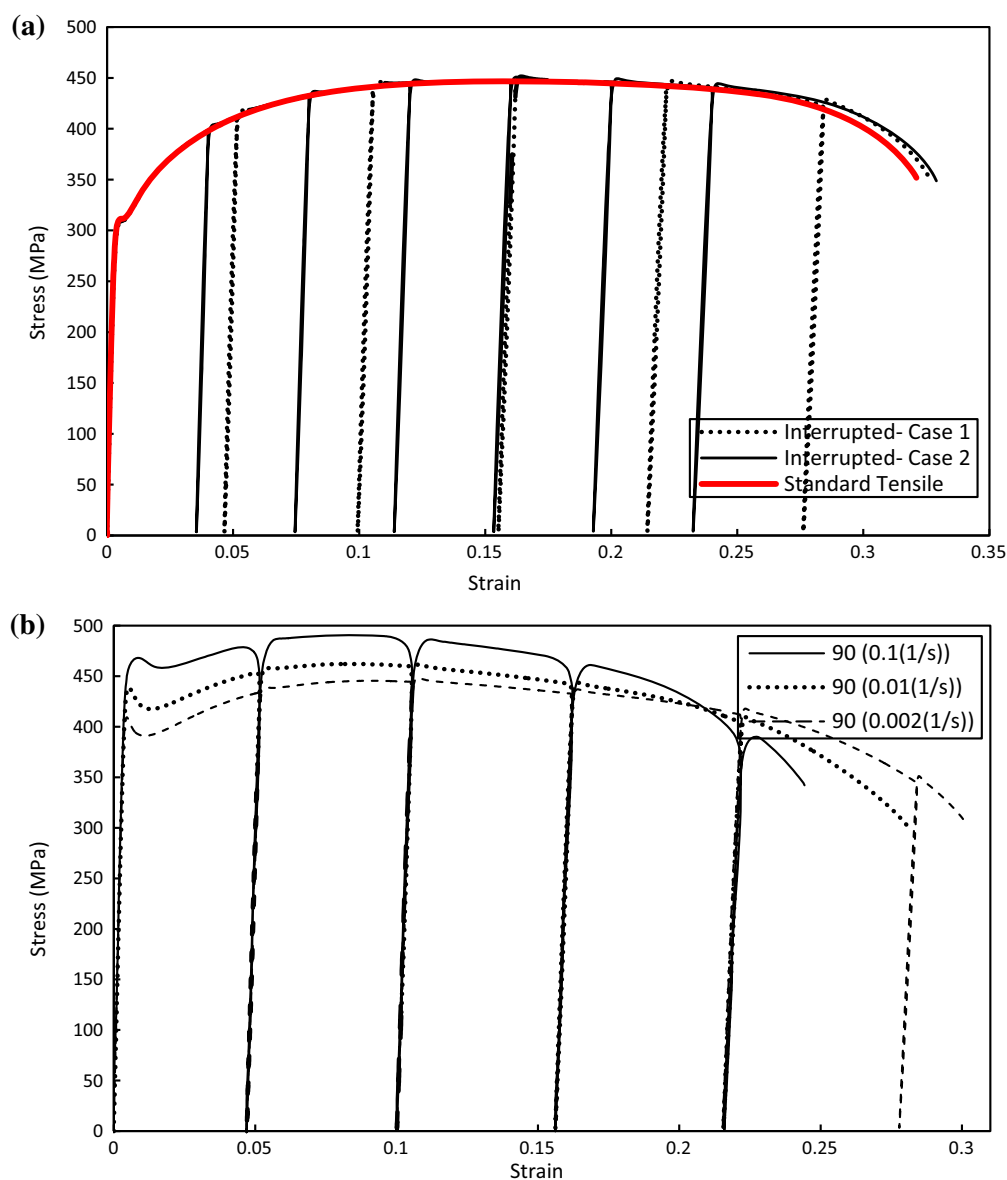

Figure 6 a Engineering stress–true strain curves for two interrupted (i.e. sequential loading–unloading) tests on samples at 0° to the RD and under the strain rate of 0.002 s^{-1}, in which the data for a continuous tensile test are superimposed, and **b** engineering stress–true strain curves for interrupted tensile tests on samples at 90° to the RD tested under different strain rates.
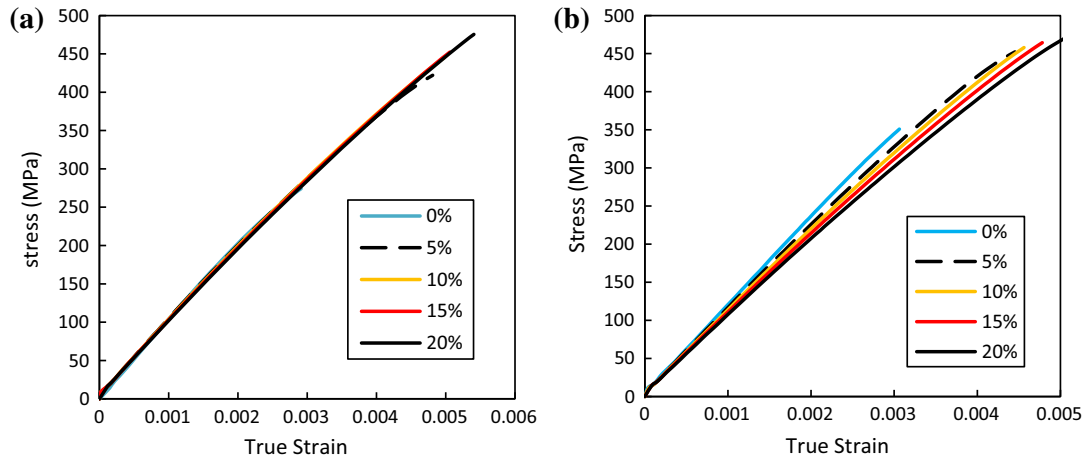
Figure 7 Engineering stress–true strain curves of the elastic regions of the loading stages of the interrupted tensile tests translated into a common reference frame, for the samples tested under $0.01\ s^{-1}$, and sample orientation at **a** 0° to the RD and **b** 90° to the RD.
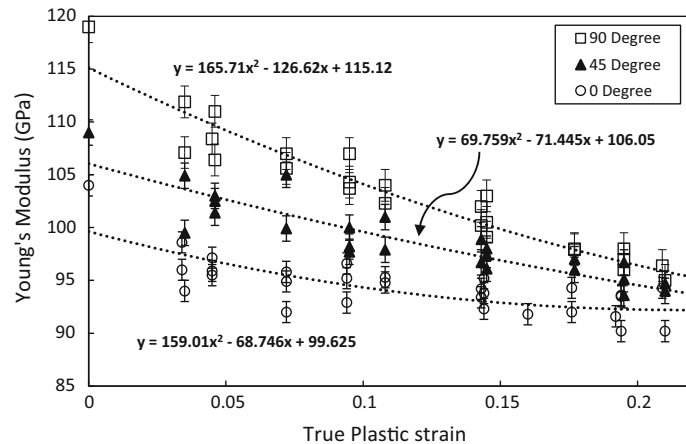

Figure 8 Degradation of Young's modulus as a function of true plastic strain for samples with different orientations to the RD.

deformation. This measurable degradation in Young's modulus is appeared to be orientation dependent, as it is more pronounced for the samples at 90° to the RD (see Fig. 7b) compared to those at 0° the RD (see Fig. 7a).

The results of interrupted tensile tests on samples with different orientations to the RD showed different levels of degradation in Young's modulus as shown in Fig. 7. This is shown in more details by plotting the degradation in Young's modulus as a function of true plastic strain for samples at 0°, 45° and 90° to the RD, in Fig. 8. For each sample orientation in Fig. 8, the presented data include the results obtained under all three strain rates (i.e. 0.1, 0.01 and $0.002\ s^{-1}$), even beyond the ultimate stress. Since the

work hardening behaviour was seen to be influenced by strain rate (see Fig. 4), the dependency of the degradation in Young's modulus on strain rate was explored. Disregarding sample orientation, these results do not show a strong dependency of degradation in Young's modulus on strain rate. Despite the higher initial elastic modulus ($\approx$ 119 GPa), the highest level of degradation in Young's modulus ($\approx$ 20%) is measured for the samples at 90° to the RD compared to those of the samples at 0° and 45° to the RD. The lowest level of degradation in Young's modulus is measured for the samples at 0° to the RD with almost 13GPa reduction from the initial measured value of 104GPa (i.e. $\approx$ 12%). This is evident in Fig. 8 where the slope of reduction in Young's

modulus rises by changing the sample orientation from 0° to 90° to the RD. All directions exhibited a substantial decrease in Young's modulus by plastic deformation and reached almost a similar value of 95GPa after ≈ 0.2 true plastic strain (Fig. 8).

Anelastic strain recovery

The nonlinear anelastic recovery occurs on unloading during each cycle of the interrupted tensile tests where the unloading curve does not appear to follow an expected Young's modulus linearly considering the degradation in Young's modulus. As discussed earlier, the Young's modulus degrades as a function of the level of plastic deformation (see Fig. 8).

Figure 9a, b shows magnified views of unloading–loading stages for two separate loops of an interrupted tensile test on a sample at 0° the RD and under strain rate of 0.01 s^{-1}. The unloading curve for loop 1 (see Fig. 9a) follows the straight Young's modulus (≈ 105GPa) line on unloading down to just below 200 MPa stress and then deviates from the elastic recovery line by an additional nonlinear recovery. This type of nonlinear recovery was observed for all steps during the interrupted tensile tests.

Figure 9b shows a similar nonlinear recovery for loop 4 of the same test. For all cases, the anelastic recovery occurred when the stress dropped below ≈ 150 MPa on unloading. A noticeable reduction in the final strain, expected based on the initial Young's modulus, was measured on complete unloading. The total springback (i.e. strain recovery) on unloading can then be divided into three segments caused by elastic recovery (considering initial value), degradation in Young's elastic modulus and anelastic recovery. These are denoted as A, B and C, respectively, in Fig. 9b. Hence, the total springback can be formulated as the relationship shown in Eq. (2):

$$\varepsilon_{\text{Springback}} = \varepsilon_A + \varepsilon_B + \varepsilon_C = \frac{\sigma}{E_0} + \varepsilon_B + \varepsilon_C \qquad (2)$$

where ε_A, ε_B and ε_C are the magnitudes of strain recovered by elastic recovery, degradation in Young's modulus and anelastic recovery on unloading, respectively. ε_A, segment A in Figure 9b, can simply be computed using the Young's modulus of the as-received material with no plastic deformation. This
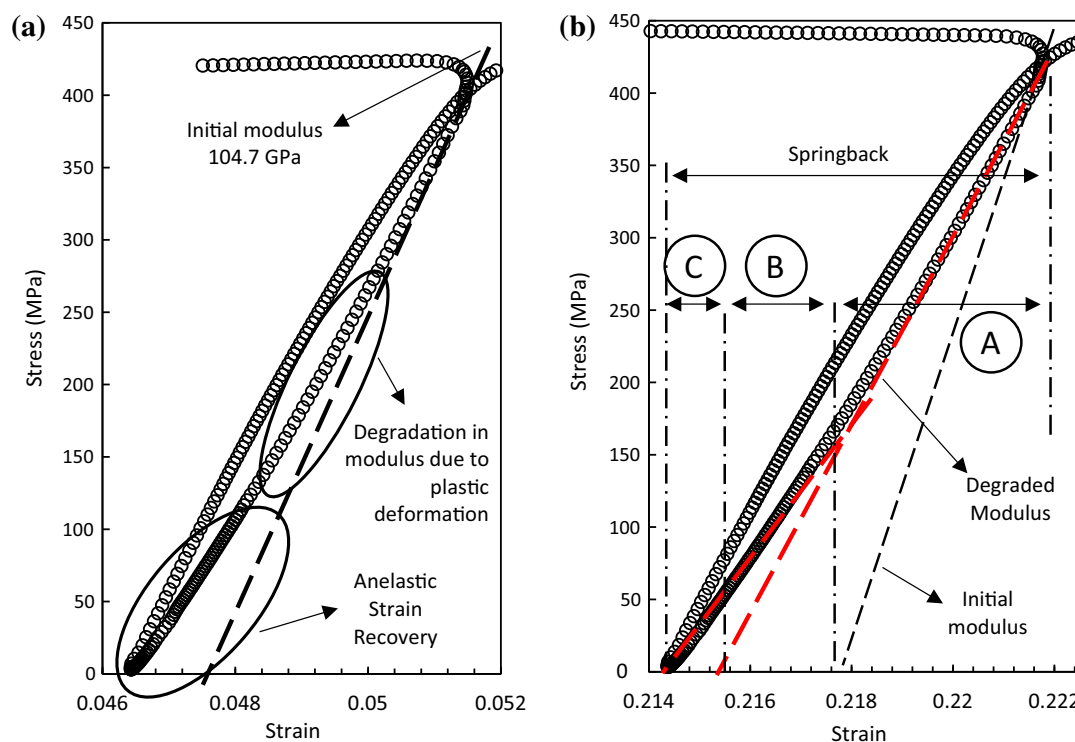

Figure 9 Typical views of the strain recovery behaviour on unloading from different levels of plastic deformation for a sample at 0° to the RD tested under strain rate of 0.01 s^{-1}, **a** after ≈ 0.05 and **b** after ≈ 0.2 true plastic strains, corresponding to loop 1 and loop 4 of the interrupted tensile test.
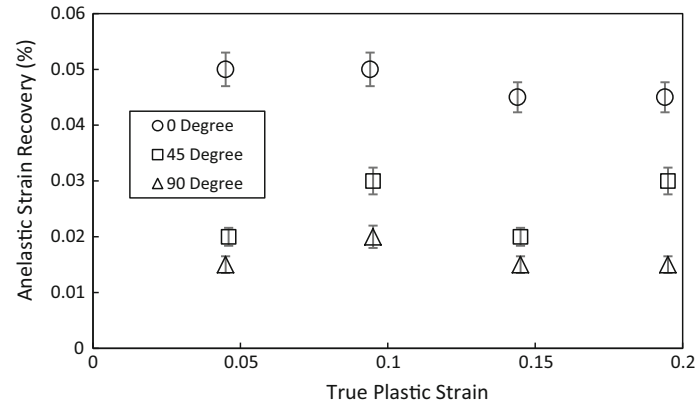
Figure 10 Anelastic strain recovery of samples with different orientations with respect to the RD as a function of true plastic strain and under strain rate of 0.01 s^{-1}.

can be different for different sample orientations in anisotropic materials such as the CP-Ti material studied in this work (see Table 1), in which case the magnitude of computed elastic strain recovery (i.e. segment A in Fig. 9b) is not identical for different sample orientations. ε_B, segment B in Fig. 9b, is caused by the degradation in the Young's modulus as a function of plastic deformation as shown in Fig. 8. ε_C, segment C in Fig. 9b, is a springback which is caused by nonlinear strain recovery.

The plot of nonlinear strain recovery (ε_C) evolution as a function of plastic strain for all sample orientations is shown in Fig. 10 for the tests conducted under 0.01 s^{-1} strain rate. The magnitudes of nonlinear strain recovery for the samples at 0° to the RD are observed to be higher by an order of magnitude (≈ 0.0005) than those of the samples at 45° and 90° to the RD. The magnitudes of anelastic strain recovery for samples at 45° and 90° to the RD are almost in the same range, with those of the former slightly higher than those of the latter. The magnitude of nonlinear strain recovery as a function of plastic deformation remained almost constant for all directions, under a constant strain rate. Therefore, the magnitude of nonlinear strain recovery appears to be directional dependent with respect to the orientation of the as-received sheet. A similar evaluation approach for all sample orientations under different strain rates of 0.1 and 0.002 s^{-1} showed that the magnitude of nonlinear strain recovery is independent of applied strain rate.

As shown in Fig. 9, the material shows a complex nonlinear strain recovery behaviour following unloading from stresses corresponding to different levels of plastic deformation. To further investigate this behaviour, the instantaneous tangent modulus ($d\sigma/d\varepsilon$) of the unloading segment of the loading–unloading loops for all the interrupted tensile tests are calculated and plotted in a common origin in a same coordinate system. These data are shown in Fig. 11a, b and c as functions of true plastic stress to evaluate effects of strain rate, level of plastic deformation and sample orientation, respectively. Figure 11a shows the results of these calculations for the samples at 0° to the RD that were deformed to 0.05 plastic strain under different strain rates of 0.1, 0.01 and 0.002 s^{-1}. For all cases, the instantaneous tangent modulus curve, plotted as a function of true stress, can be divided into two sections of (1) linear, starting from high stress values and ending at ≈ 150 MPa, and (2) nonlinear, where the slope of the curves alters drastically with higher gradients. The change in the slope is coinciding with a point where the nonlinear strain recovery is commenced (see Fig. 9), which is typically around 150 MPa stress. Figure 11a also shows that disregarding strain rate, the first section of the instantaneous tangent modulus as a function of true stress curve decreases with a similar slope.

Figure 11b shows the instantaneous tangent modulus as a function of true stress for different unloading cycles of an interrupted tensile test. A decrease in the slope of the initial linear section of the instantaneous tangent modulus is observed with an increase in the level of plastic strain (see Fig. 11b). However, the slopes of these curves at lower levels of true stress are identical for all different levels of plastic strains. This behaviour is in a good agreement with the observed degradation in Young's modulus
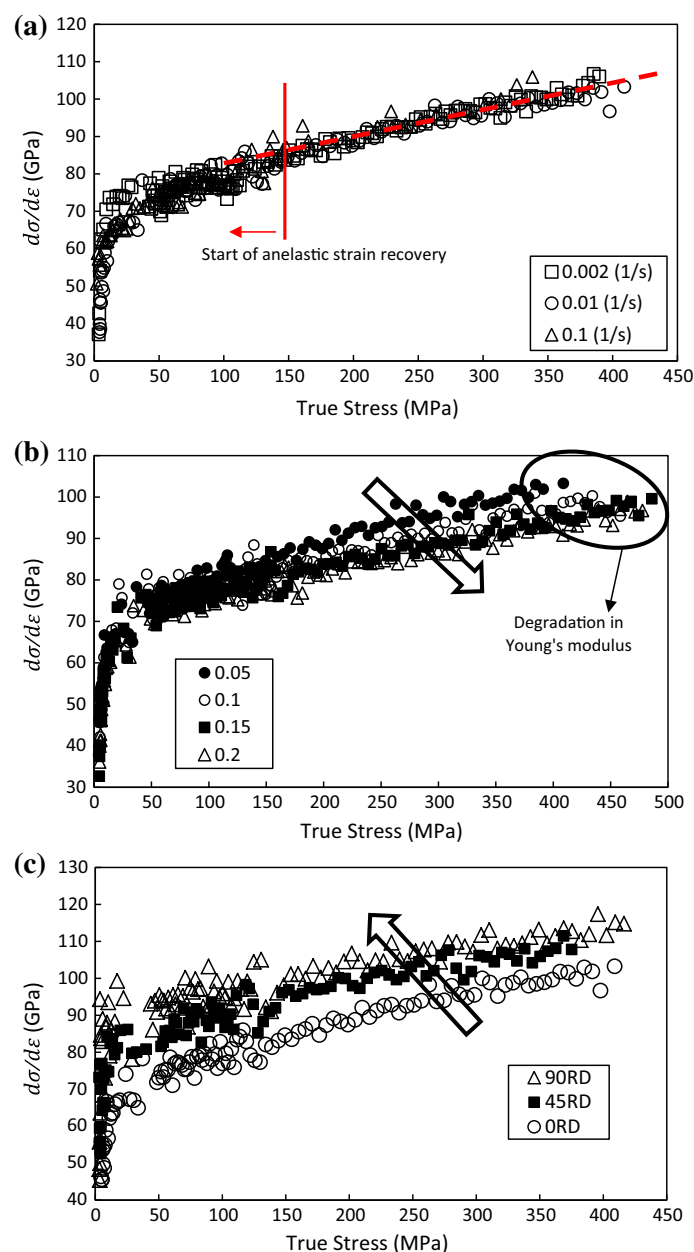
Figure 11 Evolution of instantaneous tangent modulus (dσ/dε) as a function of true stress during unloading stage of interrupted tensile tests carried out on CP-Ti50A. **a** Samples aligned with the RD underwent 0.05 true plastic strain under different strain rates. **b** Sample 0° to the RD subjected to different levels of true plastic strain (i.e. different loops of the same interrupted tensile test) under constant strain rate of 0.01 s^{-1}. Note that the data for unloading stage of all loops are transferred to a common coordinate system with the same origin. **c** Samples with different orientations with respect to the RD underwent 0.05 true plastic strain with constant strain rate of 0.01 s^{-1}.

as a function of plastic deformation discussed earlier (see Fig. 8). Figure 11c shows the instantaneous tangent modulus curves as a function of true stress for tests conducted on different sample orientations under the same strain rate of 0.01 s^{-1}. These data are only shown for the first loop of the interrupted tensile tests, where the samples were deformed to 0.05 true

plastic strains. The data suggest that the slope of the instantaneous tangent modulus increases by changing the sample orientation from 0° to 90° to the RD. This is primarily due to the fact that the initial Young's modulus of the material at 90° to the RD is higher than that of the sample at 0° to the RD (see Table 1).

Discussion

In-plane springback in CP-Ti50A

The titanium used in this study exhibited anisotropic mechanical behaviours for different sample orientations with respect to the RD, as shown in Fig. 5. This heterogeneity in the mechanical behaviour as functions of sample orientation and strain rate will consequently influence the final springback, following sheet forming processes. The experimentally measured residual stresses, shown in Fig. 3, indicate the existence of negligible residual stress in the manufactured samples prior to the mechanical testing. This agrees with the assumption that the measurement of springback has not been influenced by residual stress.

The measured springback during unloading, using both DIC and external extensometer, has been evaluated for all samples to understand the effect of sample orientation and strain rate on springback during uniaxial tensile tests. Figure 12a, c, e shows the variation of measured springback as a function of plastic deformation on samples with different orientations to the RD, under constant strain rates of 0.002, 0.01 and 0.1 s^{-1}, respectively. Overall, the level of springback is increased with higher levels of plastic deformation for all sample orientations. The samples at 45° and 90° to the RD show lower magnitudes of springback compared to those at 0° to the RD. The origin of this significant difference is in the higher nonlinear strain recovery of the samples aligned with the RD, as shown in Fig. 10. The order of variation in springback between different sample orientations remains approximately the same for all the applied strain rates. The influence of strain rate on springback is shown in Fig. 12b, d and f, respectively, for samples at 0°, 45° and 90° to the RD. Overall, it can be seen that the springback increases for all sample orientations by an increase in the strain rate.

The results presented in Fig. 12 are in line with the findings reported elsewhere for different materials [25–27]. It was argued by Kulkarni and Prabhakar [27] that strain rate dependency of springback is different for different materials. This is discussed for two types of aluminium alloys where type 2024-T3 was more sensitive to strain rate compared to type 2024-O. For the CP-Ti-50A material used in this study, strain rate sensitivity was observed (see Fig. 12). The specimens at 45° to the RD showed the

highest sensitivity to strain rate (see Fig. 12d) compared to those of the samples at 0° and 90° (see Fig. 12b, f) which are almost half in magnitude.

Springback characterisation

The results of the present study show that in addition to material's anisotropic mechanical properties and strain rate dependency, the degradation in Young's elastic modulus as a function of plastic deformation and also the anelastic strain recovery are crucially important factors in predicting springback. These are shown schematically in Fig. 13, where segments A, B and C represent different parts of springback, as illustrated in experimentally in Figure 9. Therefore, accurate prediction of springback in this material requires several considerations that are discussed in the following.

1. Strain rate dependency of the flow behaviour of the material [15, 25–27]: as shown in Fig. 4, the Ti-50A grade used in this study showed a noticeable strain rate dependency. During sheet metal forming processes, depending on the complexity of the desired geometry, the material undergoes heterogeneous plastic deformation with different strain rates [15, 25–27]. This can influence springback as shown experimentally over a wide range of strain rates and for different sample orientations in Fig. 12.

2. Degradation in Young's modulus with progress of plastic deformation [1, 5–11, 13–19]: as shown in Figure 8, the degradation in Young's modulus is significantly high which is orientation dependent. The measured degradations in Young's modulus were 20% for the samples at 90° to the RD at highest and 13% for those at 0° to the RD at lowest, and those of the samples at 45° to the RD were in between. Similar results are reported from a study conducted on deep drawing of quality special killed (DQSK) steel [1] where the highest level of degradation in Young's modulus was observed for the samples at 0° and 90° to the RD, and the lowest was observed for those at 45° to the RD. Results from previous studies gained from different materials such as dual-phase steels (i.e. DP500, DP600, and DP780) [19], pure iron [11] and TRIP 700 steel [7] showed different levels of degradation in Young's modulus for different materials.
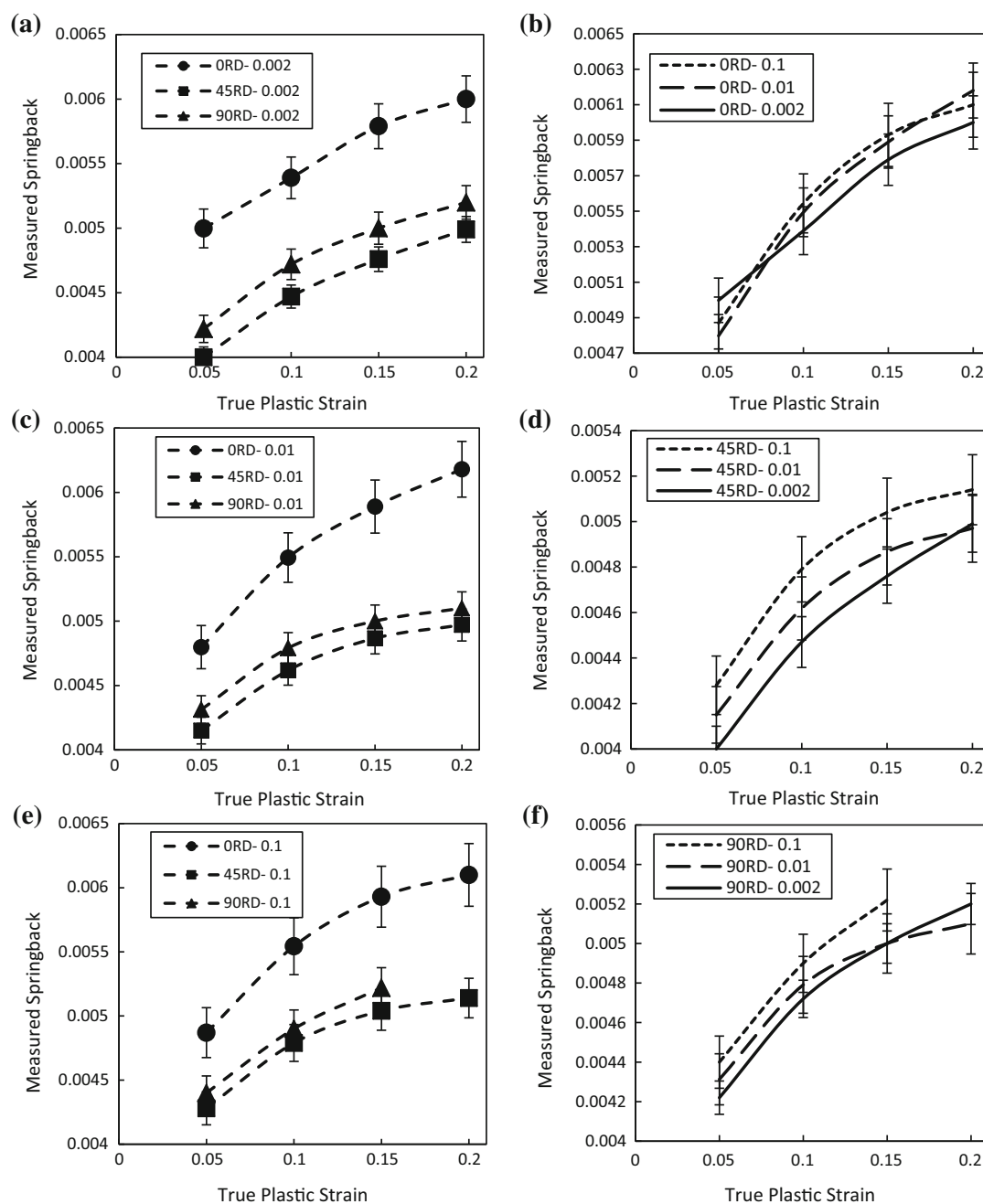
Figure 12 Measured springback during unloading stage of interrupted tensile tests, as a function of true plastic strain, for **a**, **c** and **e** constant strain rates and different sample orientations (i.e. 0°, 45° and 90° to the RD), and **b**, **d** and **e** identical sample orientations and different applied strain rates.

3. Anelastic strain recovery (i.e. segment C in Fig. 13) during unloading [6, 14, 18]: In the present study, it was shown that the anelastic strain recovery contributed ≈ 10% in the total springback for samples at 0o to the RD. The presented results suggest that this behaviour is orientation dependent (see Fig. 10). Neglecting

segment C in Fig. 13 (i.e. anelastic recovery) would result in inaccurate estimation of springback, as this has not often been considered in existing studies on springback reported in the literature [1, 8, 9, 11].

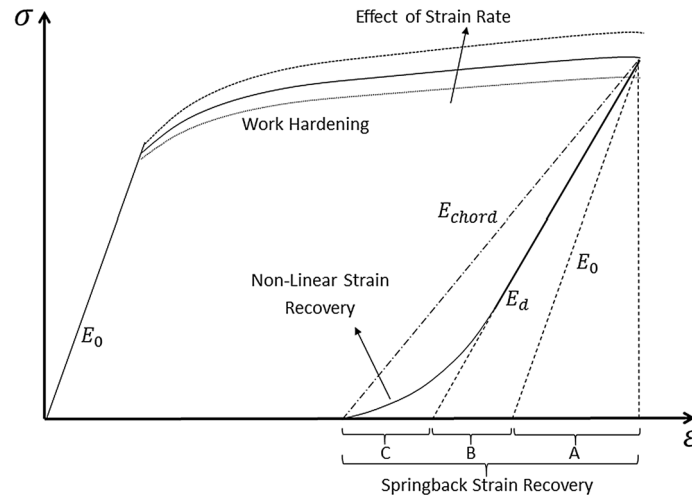4. Anisotropic material behaviour: as shown in Fig. 12, different levels of springback occurred

Figure 13 Schematic illustration of elastic and anelastic strain recovery during applied load removal leading to springback. The degradation in Young's elastic modulus has also been schematically shown as the deviation of the elastic modulus (E_d) from the initial elastic modulus (E_0).

for different sample orientations. These results are in agreement with a number of studies evaluated the effects of anisotropic mechanical properties on springback [7, 28–30]. Therefore, it is imperative to consider materials anisotropic behaviour, to estimate springback accurately. The anisotropic materials behaviour and the measured decrease in the Young's modulus with a progress of plastic deformation are due to the presence of relatively strong texture and preferred crystallographic orientation of the CP-Ti material used in this study. The IPF coloured EBSD map (see Fig. 1) shows a fairly strong alignment of {0001} poles, i.e. the c-axis of the HCP α unit cell, towards TD as suggested by the presence of dominant red (or close to red) coloured grains within the microstructure. As shown in Fig. 1c, the {0001} poles are oriented along a direction at ± (25°–30°) from the ND towards the TD and perpendicular (i.e. at 90° angle) to the RD. This explains the difference in the measured Young's modulus for the sample orientation at 0° to the RD compared to that at 90° to the RD (see Table 1). Nevertheless, anisotropic mechanical behaviours are expected for textured titanium, especially at room temperature. Furthermore, noticeable difference also exists for the 0.2% proof strength, whilst the ductility is not strongly influenced by texture at room temperature (see Table 1).

Chord modulus

As discussed, the occurrence of springback in uniaxial direction consists of two sections of linear (i.e. elastic strain recovery) and anelastic strain recovery (see Fig. 13). Recent studies [5–7, 9, 10, 13, 14, 24] have shown that Chord modulus, that is the slope of a straight line connecting the start and end points of the unloading curve (see Fig. 13), is a good estimation of average springback including both the degradation in Young's modulus and anelastic strain recovery. Chord modulus has been used in springback prediction models based on finite element analyses [5, 10, 14], and the results were more closer to the experimentally measured springback. A similar approach was implemented by Chen et al. [5] where four separate values were considered for elastic modulus to describe the changes throughout a loading–unloading loop. These four values were the slopes of the stress–strain curves at the beginning and the end of loading and unloading curves, denoted as E1, E2, E3 and E4, respectively. It was argued that E1 and E3, and E2 and E4 are almost identical, and the Chord modulus is very close to the average of all these four quantities [5].

Chord modulus is computed for the interrupted tensile tests conducted in this study, and the results are shown in Fig. 14 along with the measured Young's modulus as functions of plastic deformation. Figure 14 shows the data for 0° and 90° to the RD sample orientations, as the two extreme conditions of
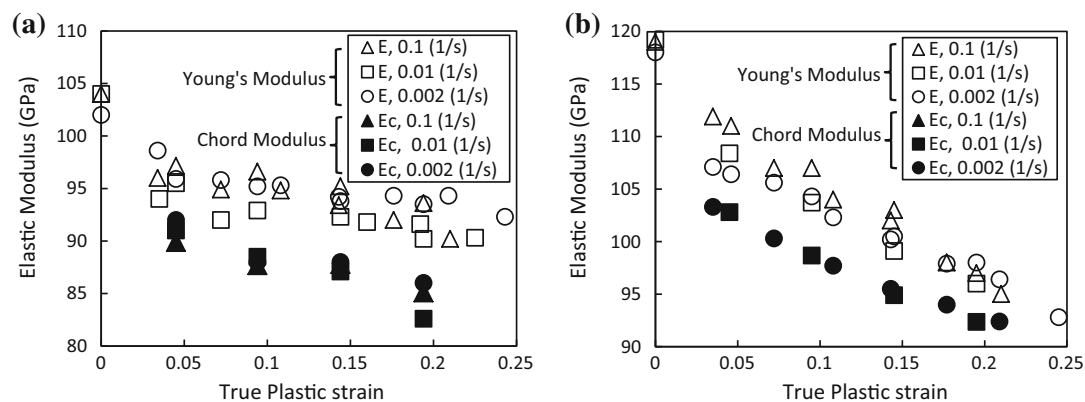
Figure 14 Degradation in Young's modulus and Chord modulus as a function of true plastic strain for tests conducted under different strain rates of 0.1, 0.01 and 0.002 s^{-1} on; **a** samples at 0° to the RD and **b** samples at 90° to the RD.

degradation under different strain rates. The initial value for Chord modulus at no plastic deformation is assumed to be equal to normal Young's modulus. As shown in Fig. 14, the Chord modulus was measured to be lower than Young's modulus at similar level of plastic deformation. This is due to the lower slope of the unloading curve caused by anelastic strain recovery (see the schematic in Fig. 13). Similar trend of degradation is observed for Chord modulus as that of the Young's modulus, with a progress of plastic deformation. Also, similarly to the Young's modulus, the degradation in Chord modulus appears to be independent of strain rate. Similar observations have been reported for different materials [5, 8, 14].

Modelling in-plane springback

Finite element analyses were performed to simulate the uniaxial tensile testing using experimental data obtained in this study, to predict springback upon removing load after certain level of plastic deformations. Data obtained for different sample orientations (see Fig. 4 and Table 1) were used to evaluate the magnitude of springback in different orientations. The material behaviour is modelled by implementing the flow curves of material in the format of true stress–true plastic stain for each strain rate. A similar procedure was applied for each sample orientation. In these simulations, the degradation in Young's modulus has been taken into consideration. The applied boundary conditions were in a way that one side of the uniaxial sample was restricted to move in vertical direction (i.e. Y) and free to move in horizontal direction (i.e. X). Extension in the gauge length that was aligned with the Y direction was applied

through displacements to the top edge of the uniaxial sample along Y. The degradation of Young's modulus as a function of plastic deformation (see Fig. 8a was implemented using a USDFLD subroutine. Simulations were also performed to predict springback by taking the calculated Chord modulus (Fig. 14) into account instead of Young's modulus. These simulations were conducted in ABAQUS by using 8-node linear brick (C3D8) element type.

Figure 15a and b, respectively, shows the results of simulations for two sample orientations of parallel and perpendicular to the RD, under applied strain rate of 0.01 s^{-1}. The experimentally measured springback data are also provided for the aid of comparison. The results are also shown for the simulations with and without considering the degradation in elastic modulus and those with considering the Chord modulus. It can be seen, for both sample orientations, without considering the degradation in Young's modulus in the simulations, the predicted springback is significantly lower than the experimental results. On the other hand, by considering the degradation in Young's modulus as a function of plastic deformation in the simulation, the predicted springback is improved. However, there is still a gap between the results of prediction models and the experimentally measured springback. This can be due to the observed nonlinear strain recovery (see Fig. 10) that has not been taken into consideration in the prediction model. In an attempt to consider both the degradation in Young's modulus and anelastic strain recovery in the simulation model, Chord modulus was implemented. Note that the degradation in Chord modulus with a progress of plastic
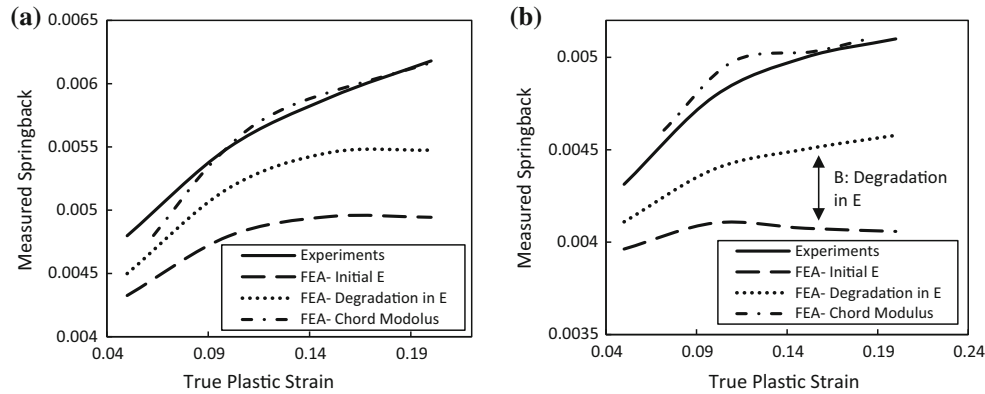
Figure 15 Comparison between experimentally measured springback and the results of FE simulations. The FE simulations are carried out with and without considering the degradation in Young's modulus and also with Chord (E_{Chord}) modulus. **a** Samples at 0° to the RD and **b** samples at 90° to the RD, under strain rate of 0.01 s^{-1}.

deformation, as shown in Fig. 14, is also considered. By repeating the simulations on these bases, the results of FE predictions become significantly closer to the results of measured springback. Similar improvements in the predicted data were observed for other sample orientations and applied strain rates. This shows that the springback can be evaluated with reasonably small uncertainties when considering the Chord modulus. However, due to the anelastic behaviour, the linear unloading section cannot be estimated accurately with Chord modulus. This will be also pronounced for complex forming process (i.e. sheet forming process) where different locations of the part are at different stress status.

Conclusions

In this study, detailed analyses of degradation in Young's elastic modulus and anelastic strain recovery as functions of plastic deformation, along with anisotropic mechanical behaviours in a commercially pure titanium type CP-Ti50A, were investigated. The major purpose of this study was to identify the factors contributing into springback during sheet metal forming, and the major observations are concluded as follows:

- Degradation in Young's modulus is observed as a function of plastic deformation which is dependent on sample orientation and independent of strain rate. The highest level of degradation in Young's modulus was measured to be ≈ 20% for

samples perpendicular to the RD compared to ≈ 13% for those aligned with RD.
- Anelastic strain recovery, that is an element of springback, was observed during unloading which is directional dependent. The highest level of anelastic strain recovery (≈ 10% of the total springback) was measured for the samples with their length along the RD.
- The magnitude of anelastic strain recovery is almost equal to the level of strain recovery caused by the degradation in Young's modulus as a function of plastic deformation.
- The level of measured total springback differs for different directions and increases by increasing strain rate during plastic deformation.
- The Chord modulus is found to be more efficient in predicting springback, especially for uniaxial loading–unloading tests. This modulus is able to reasonably estimate the strain recovery caused by both the degradation in Young's modulus and also the anelastic strain recovery. However, Chord modulus is not efficient in predicting the elastic recovery (segments A and B) only.

Acknowledgements

References

[1] Luo L, Ghosh AK (2003) Elastic and inelastic recovery after plastic deformation of DQSK steel sheet. J Eng Mater Technol 125(3):237

[2] Eglin JC, Gouty O, Joanna D (1996) Shape and process parameters optimization for the accurate control of springback in sheets metal forming. In: Sheet metal, vol 2. University of Twente, Enschede, pp 3–14

[3] Joannic D (998) Modelisation mecanique et simulation du retour elastique en emboutissage des toles minces et optimisation parametrique. Ph. D. thesis, Université de Franche-Compté, Besançon

[4] Burchitz IA (2008) Improvement of springback prediction in sheet metal forming. Netherlands Institute for Metals Research, Delft

[5] Chen Z, Gandhi U, Lee J, Wagoner RH (2016) Variation and consistency of Young's modulus in steel. J Mater Process Technol 227:227–243

[6] Chen Z, Bong HJ, Li D, Wagoner RH (2016) The elastic–plastic transition of metals. Int J Plast 83:178–201

[7] Mendiguren J, Cortés F, Gómez X, Galdos L (2015) Elastic behaviour characterisation of TRIP 700 steel by means of loading–unloading tests. Mater Sci Eng A 634:147–152

[8] Cleveland R, Ghosh A (2002) Inelastic effects on springback in metals. Int J Plast 18(5):769–785

[9] Pérez R, Benito JA, Prado JM (2005) Study of the inelastic response of TRIP steels after plastic deformation. ISIJ Int 45(12):1925–1933

[10] Abvabi A, Mendiguren J, Kupke A, Rolfe B, Weiss M (2016) Evolution of elastic modulus in roll forming. Int J Mater Form 10(3):463–471

[11] Benito JA, Manero JM, Jorba J, Roca A (2005) Change of Young's modulus of cold-deformed pure iron in a tensile test. Metall Mater Trans A 36:3317

[12] Evans M (2008) Measuring the predictive accuracy of various models of formability of Corus Tubular Blanks. J Mater Sci 43(8):2562–2573. https://doi.org/10.1007/s10853-008-2472-x

[13] Mendiguren J, Trujillo JJ, Cortés F, Galdos L (2013) An extended elastic law to represent non-linear elastic behaviour: application in computational metal forming. Int J Mech Sci 77:57–64

[14] Sun L, Wagoner RH (2011) Complex unloading behavior: nature of the deformation and its consistent constitutive representation. Int J Plast 27(7):1126–1144

[15] Kim H, Kim C, Barlat F, Pavlina E, Lee M-G (2013) Nonlinear elastic behaviors of low and high strength steels in unloading and reloading. Mater Sci Eng A 562:161–171

[16] Mendiguren J, Cortés F, Galdos L, Berveiller S (2013) Strain path's influence on the elastic behaviour of the TRIP 700 steel. Mater Sci Eng A 560:433–438

[17] Ma L, Ricker RE (2005) Effect of plastic strain on modulus and springback predictions of an aluminum alloy. In: 11th international symposium on plasticity. Kauai, Hawaii, pp 121–123, 4–8 Jan

[18] Yu HY (2009) Variation of elastic modulus during plastic deformation and its influence on springback. J. Mater Des 30:846–850

[19] Xue X, Liao J, Vincze G, Pereira AB, Barlat F (2016) Experimental assessment of nonlinear elastic behaviour of dual-phase steels and application to springback prediction. Int J Mech Sci 117:1–15

[20] Andar MO, Kuwabara T, Yonemura S, Uenishi A (2010) Elastic-plastic and inelastic characteristics of high strength steel sheets under biaxial loading and unloading. ISIJ Int 50(4):613–619

[21] Wang H, Yan Y, Wan M, Wu X (2012) Experimental investigation and constitutive modeling for the hardening behavior of 5754O aluminum alloy sheet under two-stage loading. Int J Solids Struct 49(26):3693–3710

[22] Zang S, Lee M-G, Sun L, Kim JH (2014) Measurement of the Bauschinger behavior of sheet metals by three-point bending springback test with pre-strained strips. Int J Plast 59:84–107

[23] Munitz A, Kaufman MJ (2013) Springback and anelasticity of mg alloys measured in three-point bending. J Mater Sci 48(15):5361–5372. https://doi.org/10.1007/s10853-013-7331-8

[24] Lee K-H, Kim Y-J, Jerng DW, Ainsworth RA, Dean D (2013) Creep elastic follow-up factors under combined primary and secondary stresses. Int J Press Vessel Pip 101:12–22

[25] Ghosh AK (1977) The Influence of strain hardening and strain-rate sensitivity on sheet metal forming. J Eng Mater Technol 99(3):264–274

[26] Leacock AG, Quinn S, Volk G, Mccracken D, Brown D (2015) The influence of strain rate on the springback of

commercially pure titanium in a stretch forming operation. Key Eng Mater 639:107–114

[27] Kulkarni P, Prabhakar S (2003) Influence of the effect of strain rates on springback in aluminum 2024 (ISO AlCu4Mg1). In: 4th European LS-DYNA users conference, vol 2024. pp 27–34

[28] Gomes C, Onipede O, Lovell M (2005) Investigation of springback in high strength anisotropic steels. J Mater Process Technol 159(1):91–98

[29] Alexandrov S, Hwang Y-M (2009) The bending moment and springback in pure bending of anisotropic sheets. Int J Solids Struct 46(25):4361–4368

[30] Nguyen V, Thomson P, Chen Z (2015) Prediction of springback in anisotropic sheet metals: the effect of orientation and friction. Proc Inst Mech Eng Part L J Mater Des Appl 229(6):503–510

[31] ASTM E8/E8M-11 (2012) Standard test methods for tension testing of metallic materials

[32] ASTM E111-04 (2010) Standard test method for Young's modulus, tangent modulus, and chord modulus. Practice, vol 3, no. Reapproved 2010, pp 1–7

[33] Fitzpatrick ME, Fry AT, Holdway P, Kandil FA, Shackleton J, Suominen L (2005) Determination of residual stresses by X-ray diffraction—Issue 2. National Physical Laboratory, Teddington, UK

[34] Zhongping Z, Weihua W, Donglin C, Qiang S, Wenzhen Z (2004) New formula relating the yield stress–strain with the strength coefficient and the strain-hardening exponent. J Mater Eng Perform 13(4):509–512